Journal of The Electrochemical Society, **150** (4) A493-A498 (2003)
0013-4651/2003/150(4)/A493/6/$7.00 © The Electrochemical Society, Inc.

High-Peak-Power Polymer Electrolyte Membrane Fuel Cells

Chunsheng Wang*,z and A. John Appleby*

Center for Electrochemical Systems and Hydrogen Research, Texas Engineering Experiment Station, Texas A&M University, College Station, Texas 77843-3402, USA

A polymer electrolyte membrane fuel cell with amorphous hydrated ruthenium dioxide ($RuO_2 \cdot xH_2O$) supercapacitative sublayers inserted between the electrocatalyst layers and the Nafion membrane was fabricated to enhance the cell's pulse power output. $RuO_2 \cdot xH_2O$ material showed a high capacitance (*ca.* 230 F/g) and allowed a much higher pulse power output, which was demonstrated by cyclic voltammetry and millisecond-width pulse voltammetry in a nitrogen atmosphere on both anode and cathode at 50°C. When the gases were changed to hydrogen and air, the sublayer slightly decreased the steady-state power output of the cell by decreasing both proton conductivity and the rate of oxygen reduction. In spite of this, the presence of the sublayer gave a much higher pulse power output, which is of value for, *e.g.*, communications applications. This modified fuel cell performs the same functions as those of a more complex fuel cell/supercapacitor hybrid system without significant increase in weight, volume, and cost. Moreover, the blocking effect of the thin RuO_2 on methanol crossover is advantageous for direct methanol fuel cell applications.
 [DOI: 10.1149/1.1559068]

Manuscript submitted August 5, 2002; revised manuscript received October 17, 2002. Available electronically February 28, 2003.

Polymer electrolyte membrane fuel cell stacks (PEMFCs) may find use in distributed cogeneration for buildings, portable power, and transportation applications because of their light weight and high power density. However, their ratio of peak to continuous power and response to instantaneous loads, *e.g.*, for communications applications and where inverters are used, is often insufficient. A typical pulse output requirement for a digital communication device is in the millisecond range. To meet such peaking requirements, the PEMFC must usually be hybridized with a supercapacitor or a high-power secondary battery.

Supercapacitors have high specific power density, rapid charging time, and are capable of many cycles, but have a low specific energy. Supercapacitors may be classified according to their mechanism of energy storage into electrical double-layer capacitors (EDLCs) and faradaic pseudocapacitors. The first stores energy by charge separation at the interface between an electrolyte electrode and a high-surface-area electrode, *e.g.*, consisting of carbon materials typically offering 40-150 F/g as single electrodes in liquid electrolyte. In contrast, faradaic pseudocapacitors use high-surface-area electroactive materials, storing energy via rapid faradaic surface reactions at the electrode-electrolyte interface. In terms of the specific energy, power, and cycle life, faradaic pseudocapacitors lie between batteries and double-layer capacitors. Amorphous hydrated ruthenium oxide ($RuO_2 \cdot xH_2O$) is a particularly attractive electrode material in a Nafion polymer electrolyte pseudocapacitor[1] because of its high stability, its relatively constant current under potentiodynamic conditions over the entire *ca.* 1.2 V aqueous window of stability, and its high specific capacitance, which reaches 720 F/g in liquid electrolytes.[2]

The PEMFC itself has double-layer capacitor characteristics because of the carbon black used as an electrocatalyst support. However, the resulting double-layer capacitance is comparatively low, typically 10-30 $\mu F/cm^2$ of real area. Thus, PEMFCs must be hybridized with a supercapacitor. Normally, fuel cell-supercapacitor hybrid systems use separate components connected by an electrical control system. This results in increased complexity, weight, volume, and cost. One solution is to incorporate the supercapacitor element into the fuel cell as a thin supercapacitive layer between the electrocatalyst and the Nafion electrolyte membrane. This is particularly effective if $RuO_2 \cdot xH_2O$ is used because of its high specific capacitance and rapid faradaic reaction. A supercapacitor based on this material internally hybridized with a PEMFC is described in which the same functions as those of a complex supercapacitor hybrid system can be performed without a significant increase in system weight, volume, and cost. Moreover, the supercapacitive sublayer also decreases methanol crossover from anode to cathode in DMFC applications, giving higher fuel efficiency and improved cathode operation.

Experimental

Preparation of gas diffusion electrodes and membrane-electrode assemblies.—In-house gas diffusion electrodes (GDEs) were fabricated using electrocatalyst-Nafion ink painted or printed on a gas diffusion layer to produce the active layer (AL) without chemical transformation of Nafion. Unless otherwise stated, an additional $RuO_2 \cdot xH_2O$ containing 54-58 wt % elemental ruthenium (Johnson Matthey, MA) supercapacitive layer (SL) was painted or printed on the AL. Platinum or Pt-Ru (50:50 atom %) nanocrystallites supported on Vulcan XC-72 conducting furnace black (E-Tek Inc., Somerset, NJ) with 20 wt % loading for pure platinum and 40 wt % for (both) Pt and Ru were used as AL electrocatalysts. Nafion (DuPont de Nemours and Company, Wilmington, DE) of equivalent weight (EW) 960 D as a 5 wt % solution (CG Solutions) was used as the perfluorosulfonate ionomer. Shawinigan acetylene black (Chevron-Texaco, Houston, TX) containing 35 wt % poly(tetrafluoroethylene) (PTFE) was spread as a thin (3 mg cm^{-2}) gas diffusion layer (GDL) on Textron (Wilmington, MA) CPW-003 lightweight carbon cloth. A flow-chart for GDE preparation is shown in Fig. 1. The electrocatalyst loadings (as Pt) were 0.17 and 0.6 mg cm^{-2}, respectively for hydrogen-air and methanol-air cell anodes, and 0.17 mg cm^{-2} for the corresponding cathodes. The amount of $RuO_2 \cdot xH_2O$ loading in supercapacitor sublayers was 4.0, or 1.5 mg cm^{-2}. Membrane electrode assemblies (MEAs) were prepared by hot-pressing the anode and cathode GDE structures symmetrically on both sides of one Nafion membrane between two 125 μm PTFE sheets (McMasterCarr, Atlanta, GA) at 70 kg cm^{-2} for 5 min at 155°C. Before pressing the MEA, the surface was impregnated with *ca.* 0.3 mg cm^{-2} ionomer by brushing with 5 wt % Nafion solution. The amount of perfluorosulfonate ionomer in the active and supercapacitive layers was 33 and 10 wt %, respectively. The schematic structure of the mutilayer electrode MEA is shown in Fig. 2. The active area of all MEAs was 1.0 cm^2, each of which was punched from a 50 cm^2 piece of MEA. Reversible hydrogen electrodes (RHEs) consisting of 5 mm diam Pt-ink-coated carbon cloth disks with 0.2 mg cm^{-2} Pt and 0.1 mg cm^{-2} 960 EW Nafion loadings were used as a reference electrode to determine PEMFC anode and cathode performance. Their centers were each at 8 mm distance

* Electrochemical Society Active Member.
z E-mail: cswang@tamu.edu

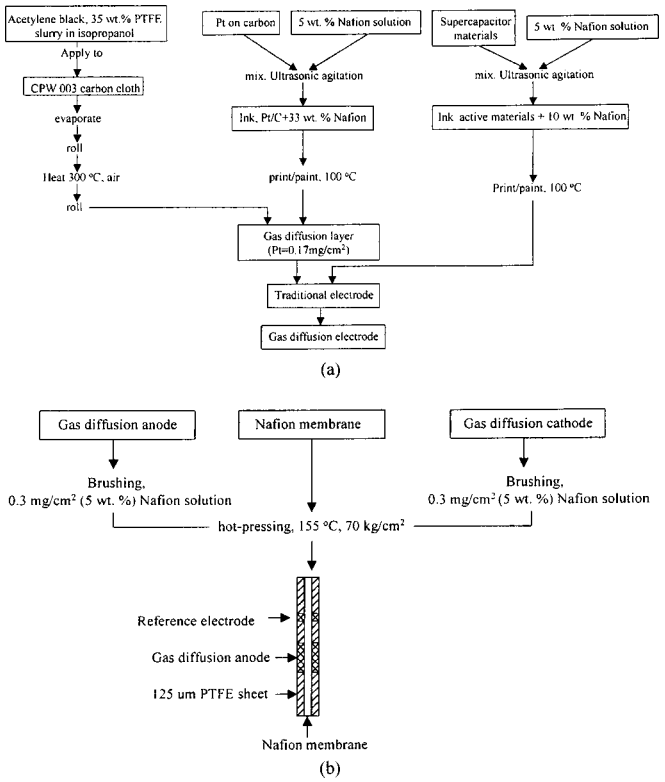

Figure 1. Preparation of (a) GDEs and (b) MEAs for high-peak-power PEMFCs.

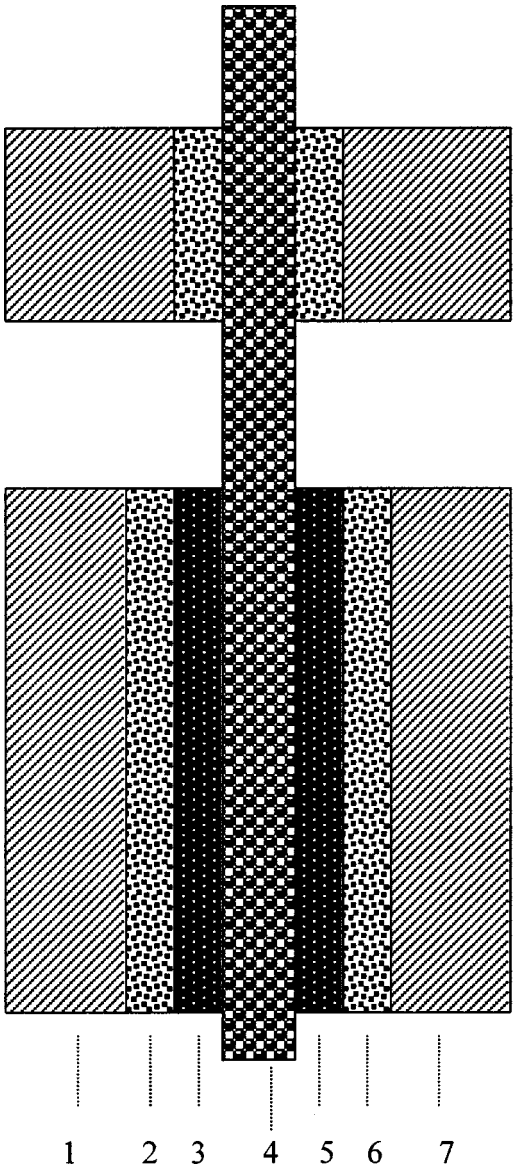

Figure 2. Schematic structure of a multilayer electrode MEA: (1) anode GDL; (2) anode electrocatalyst layer; (3) supercapacitive sublayer; (4) Nafion membrane; (5) supercapacitive sublayers; (6) cathode electrocatalyst layer; and (7) cathode GDL.

from the fuel cell electrode edges. MEA performance was evaluated by a conventional test fixture with gas flow fields consisting of Poco Carbon (Dallas, TX) graphite plates with three series-parallel ribs and channels of 0.8 mm width and depth.

Preparation of $RuO_2 \cdot xH_2O$ *supercapacitors*.—All-solid-state supercapacitors with $RuO_2 \cdot xH_2O$ active materials and Nafion electrolytes were fabricated to evaluate their capacitance and pulse power by a brushing method similar to that used for the MEAs. Active material (1.0 mg cm^{-2}) with three different quantities of Nafion ionomer (10, 30, 50 wt %) were brushed onto carbon cloth to form electrodes. The Nafion 112 membranes were hot-pressed at 135°C for 5 min using pressure of 70 kg cm^2. Before pressing the MEA, the surface was impregnated with *ca.* 0.3 mg cm^{-2} Nafion by brushing with 5 wt % solution.

Fuel cell performance measurements.—The objective of this work was not to achieve the highest cell performance but rather to evaluate the peak power output of the fuel cell with and without supercapacitive sublayers between the AL(s) and membrane. Potential-current density parameters with hydrogen and air at low utilization humidified to cell temperature were obtained using cycling voltammetry (CV) at a scan rate of 1.0 mV s^{-1} at 50°C cell temperature. The current density output of the PEMFC under pulse voltage conditions was monitored using the pulse voltammetry program shown in Fig. 3. The potential was applied as a series of pulses of 50 ms width from a constant baseline potential under load (the initial cell potential, IP), which was 0.70 V for pure hydrogen, and 0.60 V for methanol-hydrogen-water mixtures. The IP value was considered close to the normal steady-state fuel cell power output voltage. The methanol-hydrogen-water mixtures were prepared as in Jia *et al.*[3] by replacing the water in the humidifier by a 50 vol % methanol-water mixture to determine the effect of the presence or absence of SLs on methanol crossover. The pulse amplitude was progressively increased from zero to the difference between the IP and final cell potential (FP), which was 0.20 V. The potentiostat samples the current just before each new pulse and near the end of the pulse, and measures the difference between the two values. The change in pulse amplitude as a function of time was maintained the same as the CV scan rate, *i.e.*, 1.0 mV s^{-1}.

Supercapacitor performance measurements.—The charge-discharge performance of $RuO_2 \cdot xH_2O$ supercapacitors and PEMFCs with $RuO_2 \cdot xH_2O$ supercapacitive sublayers was measured using CV between −0.5 and +0.5 V at a scan rate of 20 mV s^{-1} at a device temperature of 50°C with pure nitrogen humidified to 50°C at both anode and cathode of each device. The current density output for the devices under pulse voltage conditions was measured under the same atmospheric conditions with a pulse voltammetry program similar to Fig. 3 but with an IP of 0.0 V and an FP of 0.6 V.

Electrochemical impedance spectroscopy measurements.—Electrochemical impedance spectra (EIS) as specified were

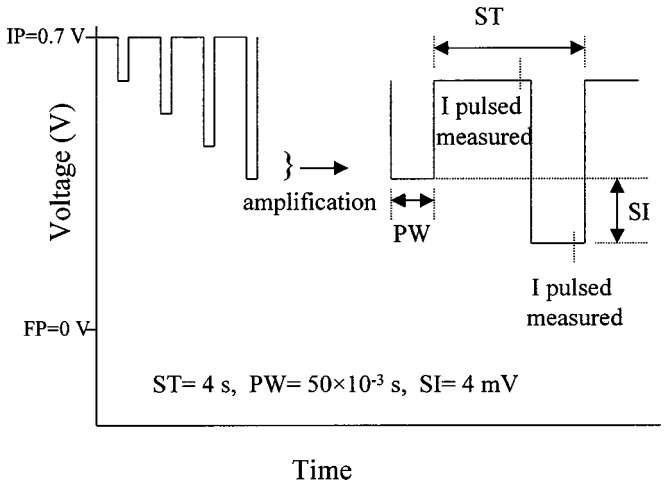

Figure 3. Pulse voltammetry program used to determine the pulse current density output of PEMFCs under pulsed voltage conditions.

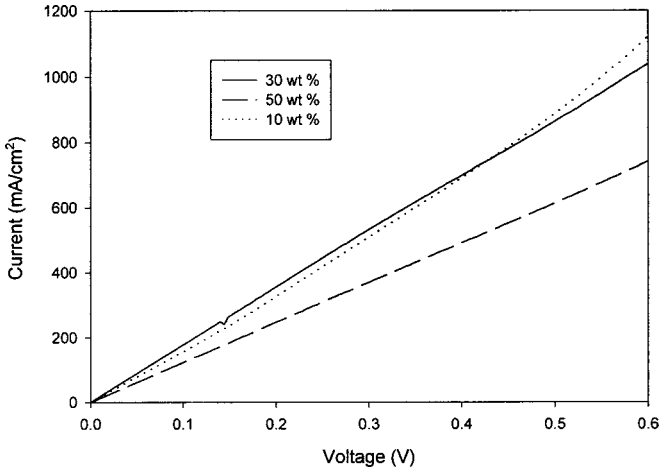

Figure 5. Pulse voltammetry of supercapacitors containing 10, 30, and 50 wt % Nafion ionomer in $RuO_2 \cdot xH_2O$ layers at 1.0 mg cm^{-2} loading.

measured from 65 kHz to 0.01 Hz at 5 mV potentiostatic signal amplitude using a Solartron 1250 frequency response analyzer and a Solartron model 1286 electrochemical interface.

Results and Discussion

Capacity of $RuO_2 \cdot xH_2O$ *supercapacitors and PEMFCs with* $RuO_2 \cdot xH_2O$ *supercapacitive sublayers*.—The structure of the all-solid-state $RuO_2 \cdot xH_2O$ supercapacitor corresponds to that of the PEMFC (Fig. 2) except for the absence of active layers. To investigate the influence of the electrocatalyst layer on the capacitive performance of $RuO_2 \cdot xH_2O$ supercapacitors, the capacitive behavior of PEM devices with and without electrocatalyst layers was measured by CV scanning (from 1.0 to 20 mV/s) and pulsed voltage scanning (1.0 mV/s) under nitrogen atmosphere on both anode and cathode sides at 50°C. Figure 4 shows the CV of a device without electrocatalyst layers (*i.e.*, a $RuO_2 \cdot xH_2O$ supercapacitor) with 30 wt % Nafion at different scan rates. CV (before activation) of the corresponding PEMFC with 0.17 mg cm^{-2} Pt loading ALs is also shown in Fig. 4 for comparison. The CV curves exhibit ideal pseudocapacitive behavior between −0.5 and +0.5 V voltage. The

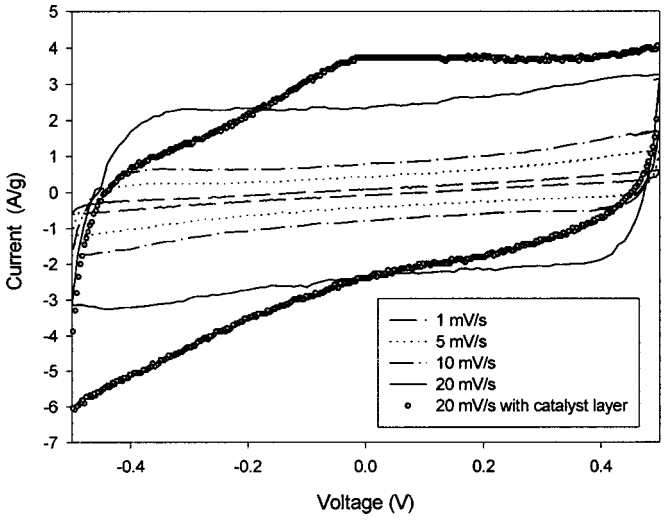

Figure 4. CV of $RuO_2 \cdot xH_2O$ supercapacitor at different scan rates. $RuO_2 \cdot xH_2O$ loading 1.0 mg cm^{-2} with 30 wt % Nafion for both anodic and cathodic sublayers.

charge and discharge currents increase linearly with scan rate, as expected. The specific capacitance c can be calculated from the CV curve via $c = i/s$, where i and s are the current and voltage scan rates, respectively. The average specific capacitance was calculated to be 230 F/g at a scan rate of 20 mV/s. This value is slightly higher than that reported by Park *et al.*,[1] but much lower than that of sol-gel $RuO_2 \cdot xH_2O$ in sulfuric acid electrolyte.[2] A possible reason for its lower capacitance in Nafion electrolyte is a smaller effective contact area between the larger RuO_2 particles and the solid polymer electrolyte. Introduction of 0.17 mg cm^{-2} Pt loading ALs between the supercapacitive and GDLs slightly increased the cathodic current (Fig. 4).

The $RuO_2 \cdot xH_2O$ layer is a mixed electronic and proton conductor. To optimize its combined electronic and proton conductivity, the capacitance of layers containing 10, 30, and 50 wt % of ionomer were examined. The effect of changing ionomer content on capacitance was small between 10 and 30 wt %, and capacity was reduced at 50 wt % loading under the Fig. 3 pulsed current conditions, as shown in Fig. 5. The capacitive current output increased linearly with pulse amplitude. The smaller current with 50 wt % ionomer is possibly due to poorer interparticle electronic contact. Since $RuO_2 \cdot xH_2O$ itself is a good electronic and proton conductor, little ionomer is required for proton conductivity. The peak current output under millisecond voltage pulse conditions is much larger than the capacitive current measured from CV, suggesting that $RuO_2 \cdot xH_2O$ has very rapid reaction kinetics. Since the current output of the supercapacitor with 10 wt % ionomer under the pulsed voltage conditions studied was slightly higher than that with a 30 wt % layer at cell voltages higher than 0.45 V (Fig. 5), an ink containing 10 wt % Nafion was used to prepare supercapacitive PEMFC sublayers after these preliminary experiments.

Performance of hydrogen/air PEMFCs with and without supercapacitive sublayers.—Figure 6 shows the steady-state and pulse load performance of a H_2/air fuel cell with different $RuO_2 \cdot xH_2O$ loadings between the electrocatalyst layer and the membrane. The results may be summarized as follows:

1. For PEMFCs without supercapacitive sublayers, the pulse current output is similar to the current at steady state for cell voltage greater than 0.5 V, becoming slightly larger below this threshold. This result suggests that the effective double-layer capacitance of the carbon black supported Pt electrocatalyst is small, giving a cell with little peaking ability.

2. While a thin $RuO_2 \cdot xH_2O$ layer between the AL and the membrane decreased the steady-state current, it increased the pulse current to almost double the continuous output. Increasing

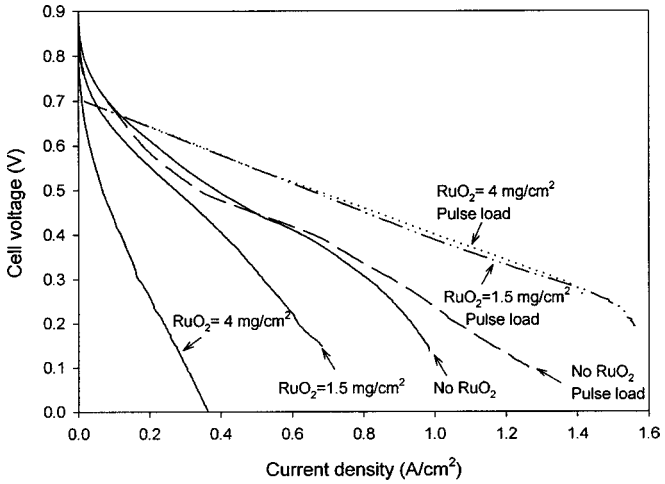

Figure 6. Performance of hydrogen/air PEMFC with different $RuO_2 \cdot xH_2O$ loadings at steady-state and pulsed loads. Steady-state performance measured by CV at 1.0 mV s^{-1}; pulse-load performance measured by the pulse voltammetry program in Fig. 3. Platinum anode and cathode electrocatalyst loading 0.17 mg cm^{-2}. Nafion 112 membrane.

$RuO_2 \cdot xH_2O$ loading decreases continuous output but has no influence on pulse current output. The energy stored in the SL is insufficient to significantly increase the continuous output measured using a CV scan rate of 1.0 mV s^{-1}, but its rapid reaction kinetics do improve PEMFC output in the form of short-duration pulses.

3. As in the solid-state supercapacitor, the pulse current output of the PEMFC with SLs increases linearly with voltage pulse amplitude.

To investigate the mechanism by which the supercapacitive sublayer decreases steady-state PEMFC current output, the impedance of the fuel cell with and without 4 mg cm^{-2} $RuO_2 \cdot xH_2O$ loading was measured at 0.6 and 0.8 V, as shown in Fig. 7. The SL increases the resistance of the cell, as the larger value of intersection of the high-frequency line with the real axis shows

Because the voltage loss in the PEMFC mainly results from oxygen cathode polarization, it must certainly be higher than that of the anode under pulsed voltage conditions, so the presence of $RuO_2 \cdot xH_2O$ on the cathode side contributes more to the pulse current than that at anode. Figure 8 shows the performance of hydrogen-air PEMFCs with supercapacitive sublayers at the anode

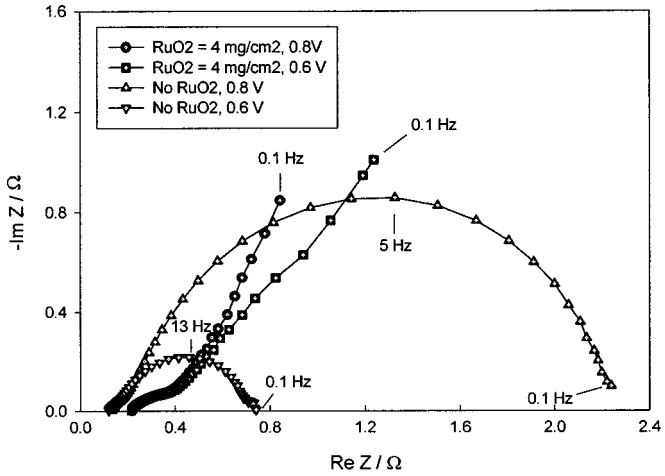

Figure 7. Impedances of hydrogen/air PEMFC with and without 4.0 mg cm^{-2} $RuO_2 \cdot xH_2O$ sublayers at 0.8 and 0.6 V cell voltages. Cell performances shown in Fig. 6. Electrocatalyst loadings as in Fig. 6.

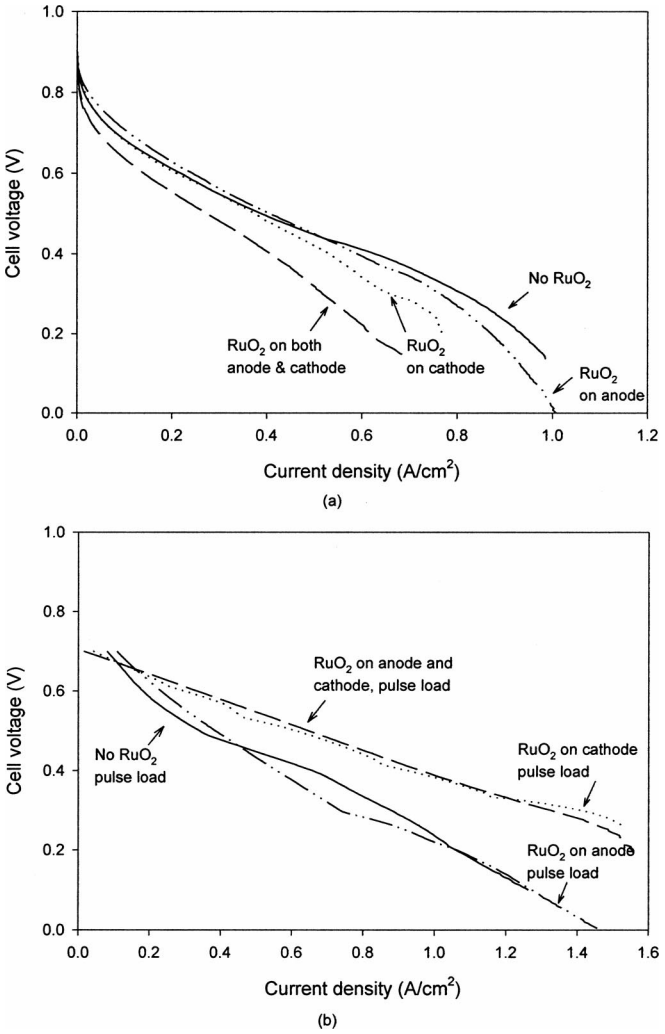

Figure 8. Performance of hydrogen/air PEMFC with 1.5 mg cm^{-2} loading $RuO_2 \cdot xH_2O$ sublayers at anode and/or at cathode side under (a) steady-state and (b) pulsed load. A similar PEMFC without supercapacitive sublayers is also shown for comparison. The performance of the PEMFC with a supercapacitive anode sublayer was measured by switching the anode and cathode after measurement the cell with the sublayer on the cathode side. Anode and cathode platinum electrocatalyst loadings 0.17 mg cm^{-2}. Nafion 112.

and/or the cathode under steady-state load and pulse power loads, with a cell without supercapacitive sublayers as a control. The steady-state output of the cells decreased as follows: with no layer $>$ with anode layer $>$ with cathode layer $>$ with anode and cathode layers. As expected, the pulse current output mainly resulted from the cathode side layer (Fig. 8b). Why the steady-state output with anode layer is higher than that with cathode layer was answered by obtaining potential-current density plots for the anode and cathode by CV at 1.0 mV s^{-1} using an RHE (Fig. 2). Figure 9 shows the anode and cathode polarization with and without supercapacitive sublayers. The performance of a cell with 1.5 mg cm^{-2} $RuO_2 \cdot xH_2O$ on the anode side was measured by switching the cathode and anode after obtaining its performance of this fuel cell with the SL at cathode side. The polarization of a cathode with a supercapacitive sublayer is higher than that without it because the layer decreases the oxygen reduction rate; however, the polarization of an anode with a supercapacitive sublayer is lower than that without it. Possible reasons for this are that $RuO_2 \cdot xH_2O$, like zirconium phosphate,[4] can retain product water when it is on the anode side, but because it has a reasonably high proton conductivity

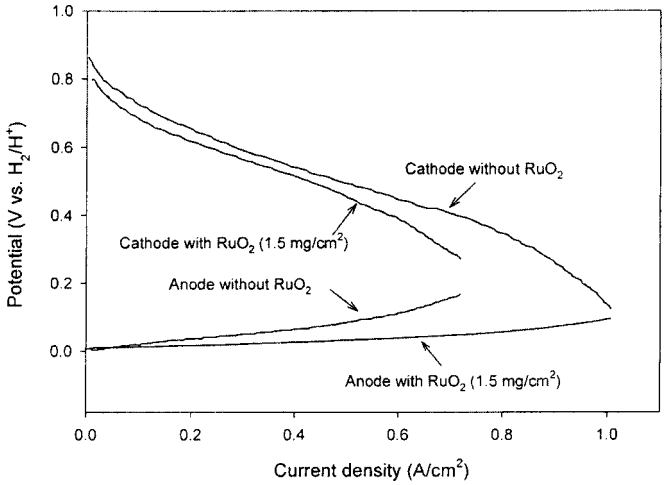

Figure 9. Anode and cathode polarization with and without supercapacitive sublayers (loading as Fig. 9).

(10^{-2} S cm^{-1} at 25°C),[5] it does not significantly interfere with proton transport, especially since water retention in an anode-side sublayer can improve local proton transport, thus decreasing anode polarization.

Although a cathode-side supercapacitive sublayer increases cathode polarization, it has a large effect on pulse current output. To improve water transport and to compensate the change in cathode kinetics with a cathode-side capacitive layer, the Nafion 112 membrane was replaced by Nafion 111 and a cathode-side $RuO_2 \cdot xH_2O$ sublayer (1.5 mg cm^{-2}). Figure 10 compares the performance of the cell with Nafion 111 and the cathode-side RuO_2 sublayer with that of the cell with Nafion 112 alone. The steady-state output of the cell with Nafion 111 and the cathode-side sublayer was similar to that of a cell with Nafion 112 without a RuO_2 capacitive sublayer, but its pulse current output was much higher.

Performance of (methanol-hydrogen)/air cells with and without supercapacitive sublayers.—With other variables remaining constant, the supercapacitive sublayer decreased proton conductivity, but it may also block methanol crossover from the anode to cathode, increasing DMFC efficiency. Results of a preliminary investigation using methanol vapor added to the hydrogen anode feedstock[3] under

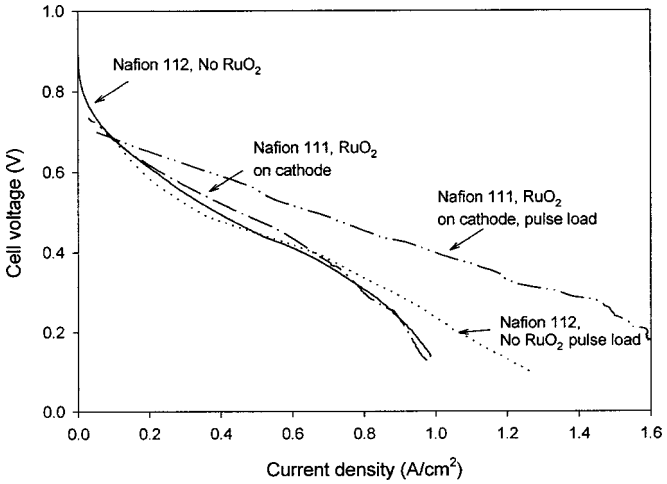

Figure 10. Performance of hydrogen/air PEMFC with SL on cathode side (loadings as Fig. 9) with Nafion 111 electrolyte. The cell with Nafion 112 without supercapacitive sublayers is shown for comparison.

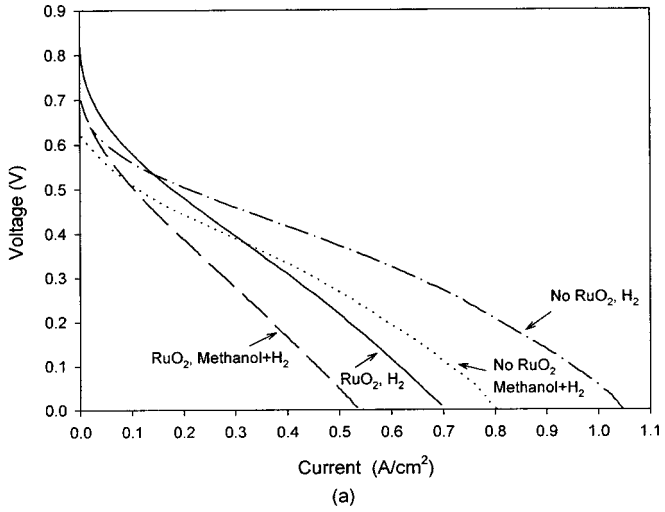

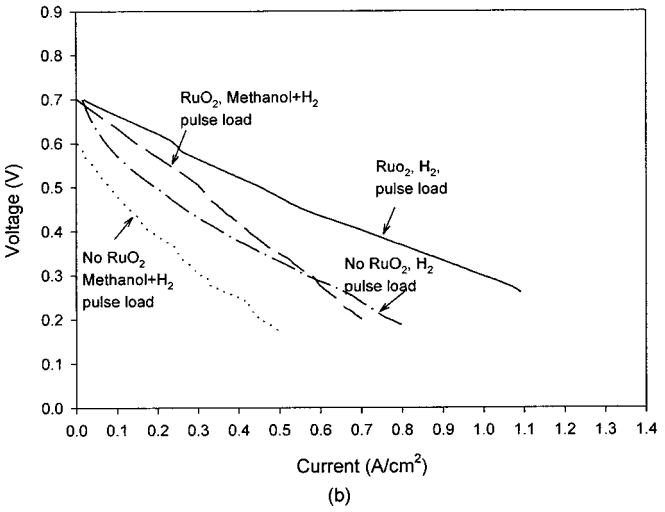

Figure 11. Voltage for methanol/hydrogen cell *vs.* current density with supercapacitive sublayers on both anode and cathode sides (loading as Fig. 9). The methanol was fed by passing hydrogen through 50 vol % water/methanol mixture at 50°C. Anode electrocatalyst (Pt_1Ru_1) loading 0.6 mg cm^{-2}, Pt cathode loading as Fig. 6, $RuO_2 \cdot xH_2O$ sublayer loadings as Fig. 9. Nafion 112 membrane.

normal and pulse voltage output are shown in Fig. 11. For steady-state output (Fig. 11a), cell performance with supercapacitive sublayers is slightly inferior to that of a cell without the sublayer. With methanol vapor added to the feedstock, the fuel cell without the sublayer is still slightly superior, but the difference between the two is less (Fig. 11a). Moreover, the pulse current output of the cell with sublayers is double that of the cell without sublayers (Fig. 11b). The effect of supercapacitive sublayers on the performance of a DMFC with 2 M liquid methanol in water fuel is currently under study.

Conclusions

High-peak-power PEMFCs were fabricated using a mixed electronic- and proton-conducting $RuO_2 \cdot xH_2O$ supercapacitive sublayer between the electrocatalyst layer(s) and the Nafion membrane. The approach resulted in a high-peak-power PEMFC that performs the same functions as those of a relatively complex supercapacitor hybrid system without significant increase in weight, volume, and cost. The thin sublayer slightly decreased the steady-state

power output of the PEMFC but doubled its pulse power output. The water retention properties of the sublayer benefits anode performance. The sublayer can somewhat decrease the methanol crossover and doubles the pulse power output of (methanol-hydrogen)/air fuel cells.

Texas A & M University assisted in meeting the publication costs of this article.

References

1. K. W. Park, H. J. Ahn, and Y. E. Sung, *J. Power Sources*, **109**, 500 (2002).
2. J. P. Zheng, *Electrochem. Solid-State Lett.*, **2**, 359 (1999).
3. N. Jia, M. C. Lefebvre, J. Halfyard, Z. Qi, and P. G. Pickup, *Electrochem. Solid-State Lett.*, **3**, 529 (2000).
4. C. Yang, S. Srinivasan, A. S. Arico, P. Creti, V. Baglio, and V. Antonucci, *Electrochem. Solid-State Lett.*, **4**, A31 (2001).
5. S. C. Thomas, X. Ren, and S. Gottesfeld, *J. Electrochem. Soc.*, **146**, 4354 (1999).